J Mater Sci (2021) 56:12596–12606

Chemical routes to materials

All-aerosol-jet-printed highly sensitive and selective polyaniline-based ammonia sensors: a route toward low-cost, low-power gas detection

Christine Fisher[1,5], Bruce J. Warmack[2], Yongchao Yu[3,4], Lydia N. Skolrood[1,6], Kai Li[1], Pooran C. Joshi[2], Tomonori Saito[1], and Tolga Aytug[1,*]

[1] Chemical Sciences Division, Oak Ridge National Laboratory, Oak Ridge, TN 37830, USA
[2] Electrification and Energy Infrastructures Division, Oak Ridge National Laboratory, Oak Ridge, TN 37830, USA
[3] Department of Mechanical, Aerospace and Biomedical Engineering, University of Tennessee, Knoxville, TN 37916, USA
[4] Manufacturing Science Division, Oak Ridge National Laboratory, Knoxville, TN 37932, USA
[5] Present address: Department of Chemistry, Virginia Tech, Blacksburg, VA 24061, USA
[6] Present address: Department of Chemical and Biomolecular Engineering, North Carolina State University, Raleigh, NC 27695, USA

Received: 28 January 2021
Accepted: 1 April 2021
Published online: 19 April 2021

ABSTRACT

We report the design and scalable fabrication of a low-cost and low-power polyaniline-based (PANI) ammonia (NH_3) gas sensor on polyimide (PI) substrates using additive manufacturing techniques. The silver interdigitated electrode (IDE) arrays and conducting polymer films are printed onto PI using a direct-write technology of aerosol-jet printing. Morphological characteristics are examined by scanning electron microscopy and energy-dispersive X-ray analysis which reveal homogeneously printed PANI film on the IDE platform. The gas sensing performance is evaluated in the analytical early leak detection range of 5–1000 ppm NH_3 in air as a function of both thermal (23 °C, 50 °C, 80 °C) and relative humidity (R_H = 0%, 30%, 50%) exposures. The sensor exhibits sensitivity down to 5 ppm NH_3 with a sub-ppm detection limit and good repeatability. We observe rapid NH_3 detection at 0% R_H with very extended times for equilibration and recovery. However, at both 30 and 50% *RH*, the room temperature response and recovery times are reduced to only about 1 min and 5 min, respectively. Experiments also reveal good sensitivity toward the analyte even at higher operating temperatures. Present results merit the practical application of aerosol-jet-printed, low-power sensors for industrial applications where low-level hazardous gas detection is essential.

Handling Editor: Maude Jimenez.

Address correspondence to E-mail: aytugt@ornl.gov

https://doi.org/10.1007/s10853-021-06080-0

GRAPHICAL ABSTRACT

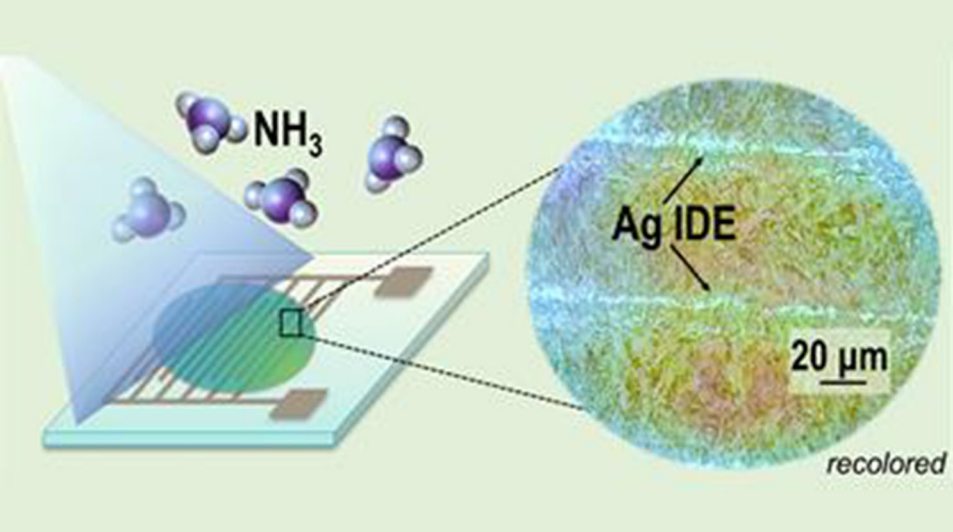

Introduction

The Environmental Protection Agency's Clean Air Act was amended in 1990 to include Title VI—Stratospheric Ozone Protection [1]. Under these changes, we have previously seen the phaseout of "Class I" chlorofluorocarbons (CFCs) which is currently being followed by the phasing out of "Class II" hydrochlorofluorocarbons (HCFCs), collectively known as Freon. A 99.5% reduction of HCFC production and consumption was mandated effective in 2020, and therefore, a pressing need exists for greener alternative refrigerants to Freon gases [2]. Compounding this issue, refrigerant gas [e.g., ammonia (NH_3)] leaks are one of the most common faults within commercial systems [3], accounting for an annual leakage rate between 11–30% [4, 5]. Management of these leaks not only results in significant economic loss but also raises health and environmental concerns [6]. Naturally derived substitutes such as hydrocarbons or NH_3 can be toxic below 50 ppm and/or flammable at concentrations of 15–28% by volume in air [7, 8] Therefore, in our progression toward emerging alternative refrigerants to HCFCs, it is crucial to develop a commercially viable early leak detection method for improved economic and safety outcomes.

With an ozone depletion potential (ODP) = 0 and global warming potential (GWP) < 1, NH_3 stands in stark contrast to typical fluorinated refrigerants (e.g., HCFC-142b ODP = 0.07, GWP = 2310) [9]. One of the most promising avenues toward widespread adoption of NH_3 as a green refrigerant relies on the advancement of chemiresistive sensors. In particular, polyaniline (PANI) has received much attention owing to its ability for rapid NH_3 detection and its relatively easy and low-cost synthesis methods [10–12]. In its conductive emeraldine salt (ES-PANI) form, NH_3 gas can abstract a proton from PANI in a reversible acid–base reaction that renders the polymer in non-conductive emeraldine base (EB-PANI) form [13]. As protonated ES-PANI retains a free polaron and positive charge, various dopants can serve as the counter-anion to significantly improve processability, as in the case of dodecylbenzenesulfonic acid (DBSA)-doped PANI, which readily forms aqueous dispersions [14]. These dispersions have been developed into inks and are being used in the development of additively manufactured gas sensors [15–17]. Accordingly, on the route toward commercialization of printed PANI-based sensors, some of the most exciting work was pioneered by Crowley

et al. where a dual-step screen-printed silver (Ag) interdigitated electrode (IDE) followed by inkjet-printed ES-PANI is employed to construct fully functional sensors with detection capabilities as low as 5 ppm [17].

In the past decade, a rapid progress has been made in the design and manufacturing of additive digital printing systems opening up a path toward an entirely new world of electronic components, devices, and systems. Among the emerging printing techniques, aerosol-jet printing enables high-resolution non-contact deposition of both the Ag electrode and PANI materials. Despite their low cost and widespread utilization, inkjet and screen printing are restricted by low spatial resolution typically to a lower limit of 30 μm for linewidth, while aerosol jets can achieve 10 μm linewidths. Previous fabrications typically have employed screen printing for electrode arrays because inkjet printers experience high rates of nozzle clogging and are limited to a narrow viscosity range near that of water (0.01–0.02 Pa-s for inkjet vs. 0.5–5.0 Pa-s for screen) [18] which also presents challenges for reproducible print quality. Because direct-write aerosol techniques allow for a wide range of ink viscosities (0.001–0.16 Pa-s) [18], the manufacturing throughput can be effectively increased as combined printing processes (e.g., screen followed by inkjet printing) are reduced to a single technique requiring minimal preparation, maintenance, and operator input. Additionally, due to the long focal length of the nozzle beam and wide distance between the nozzle and substrate in aerosol jet, prints maintaining nearly constant linewidths can be rendered on curved and textured surfaces [18]. High resolutions, good film uniformities, and streamlined manufacturing processes warrant the adoption of aerosol-jet printing for the simplified fabrication of miniaturized functional NH_3 sensing devices across various commercial applications.

Herein, to the best of our knowledge, we report the first all-aerosol-printed PANI-based NH_3 gas sensor capable of < 5 ppm sensitivity and a sub-ppm detection limit. More importantly, because of the low power consumed by the sensor (typically microwatts or less), the present approach is also promising for the advancement of miniaturized multifunctional self-powered wireless sensor platforms to realize energy efficiency and cost-saving opportunities across widespread applications. Not only are NH_3 gas sensors possessing wireless modes of operation highly desirable for residential and commercial refrigerant industries, but the mass production of these miniaturized devices may also find use as smart labels for food spoilage [19], diagnostics in kidney disease [20], and general environmental gas pollution monitors in the agricultural and automotive sectors [21]. Additionally, miniaturization not only aids manufacturing of standalone devices but is also particularly important for enabling lightweight, portable NH_3 detection instruments that may find use in tactical military operations, early warning systems for the coal mining industry, and other diverse applications.

Materials and methods

Formulation of PANI ink

The synthesis of inkjet printable DBSA-doped PANI has been previously reported and is followed [22, 23]. Briefly, 0.6 mL of fresh aniline is sonicated in 20 mL of Milli-Q deionized (DI) water for 30 min to evenly disperse the monomer. In a 125-mL round-bottom flask, 3 g of 70% (wt.%) DBSA/isopropanol is added to 20 mL Milli-Q DI water and stirred for 30 min. The aniline dispersion is slowly added to the DBSA solution while stirring, and once solvated, 0.36 g ammonium persulfate is carefully added to initiate the oxidative polymerization. The reaction is carried out at room temperature (RT = 25 °C) for 2.5 h and proceeds with the formation of brown aniline oligomers, followed by undoped blue EB-PANI, and finally, the deep emerald doped ES-PANI product. To isolate PANI nanoparticles, the reaction mixture is centrifuged at 5000 rpm for 30 min and the supernatant is collected. Further nanoparticle separation is achieved via dialysis against DI water to remove unreacted oligomers, aniline, and excess DBSA, followed by 0.1 μm pore syringe filtration. All chemicals were purchased from Sigma-Aldrich and used as received. Spectroscopic characterizations of PANI were carried out by using UV–Vis (Carry 5000) and nuclear magnetic resonance (^{1}H NMR, Bruker Avance III 400) spectroscopy (Figs. S1 and S2, respectively).

Sensor fabrication

Ag IDEs with finger and gap widths of 50 μm and 65 μm, respectively, are prepared on polyimide (PI) substrates in-house using digital aerosol-jet printing (Optomec) with the following parameters (see SV1 and SV2): nozzle print head size = 150 μm; sheath gas flow = 20 ccm; atomizer gas flow = 40 ccm; atomizer current = 0.4 mA; printing speed = 4 mm/s; and line size = 20 μm. Substrates are cured at 120 °C for 10 min on a hot plate (Torrey Pines Scientific). Two coats of PANI ink are then applied via aerosol printing to form a ~ 100-nm-thick circular film on the electrode. Morphological characterization of PANI films is performed using a Zeiss Merlin VP high-resolution field-emission scanning electron microscope (SEM) equipped with an energy-dispersive X-ray spectroscopy (EDS) unit. Figure 1a and b depicts a schematic representation and the as-fabricated NH_3 sensor, respectively. Figure 1c shows a typical morphology of PANI bridging a pair of Ag electrode fingers.

Gas sensing characterization

A custom flow-dilution apparatus is used to provide a humidity-controlled environment of NH_3 gas in air (Fig. S3). Flow controllers (MKS 1479) are used to mix bottled air (Airgas) with NH_3 prediluted to 0.2% in nitrogen (Airgas). The air is humidified as required by mixing dry air proportionately with air passed through an evaporative water boiler with a condenser controlled to approximate RT by a water recirculator. The water content of the humidified air is monitored by a chilled-mirror hygrometer (General Eastern). Colorimetric tubes (Gastec) are used to verify that the diluted NH_3 concentrations are consistent with flow dilutions. During the experiment, a 20-min presoak of NH_3 through the flow controllers is necessary to avoid retention and low concentrations of NH_3. A total flow of 400 sccm is maintained by software at all times regardless of the humidity levels and NH_3 concentrations. A PTFE hose conducts the mixed gas to a custom-machined plastic enclosure (Delrin) with an internal volume of roughly 1 mL in which the printed sensor is placed. Spring contacts connect the sample to a power supply (Agilent) typically set to 50–100 mV and a data logger (HP 34970A) to read the current (0.05–50 μA) through the sensor. Readings are automatically recorded at 10–20 s intervals. For temperature studies, the sample enclosure is placed on a temperature-controlled hotplate (Torrey Pines Scientific) and insulated with aluminum foil.

Results and discussion

The surface morphologies of the PANI films in between and on the IDE conductive traces, along with the corresponding EDS carbon and Ag elemental maps, are displayed in Fig. 2a, c, and e and Fig. 2b, d, and f, respectively. A relatively uniform coating is evident in the space between the electrodes, where the carbon yield is highly homogenous (Fig. 2a,c). On top of the electrodes the film is comparably rougher, revealing the granular structure of Ag and a relatively less intense and less uniform carbon distribution.

Sensor response, selectivity and repeatability

As defined by the National Institute for Occupational Safety and Health, NH_3 is immediately dangerous to life or health at 300 ppm level, which formed our sensor development and characterization focus. The change in resistance of the aerosol-printed PANI sensor at RT upon exposure to dry NH_3 in a logarithmically ascending series of concentrations ranging from 5 to 1000 ppm is displayed in Fig. 3.

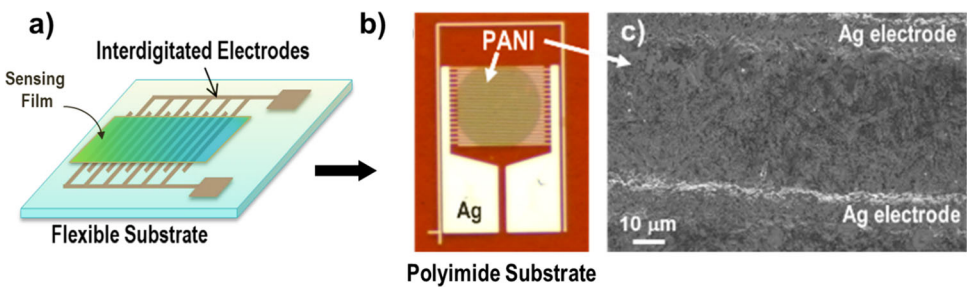

Figure 1 **a** Schematic of sensing film on interdigitated electrodes **b** as-fabricated PANI-based NH_3 gas sensor, and **c** SEM image of the PANI film on the sensing device.

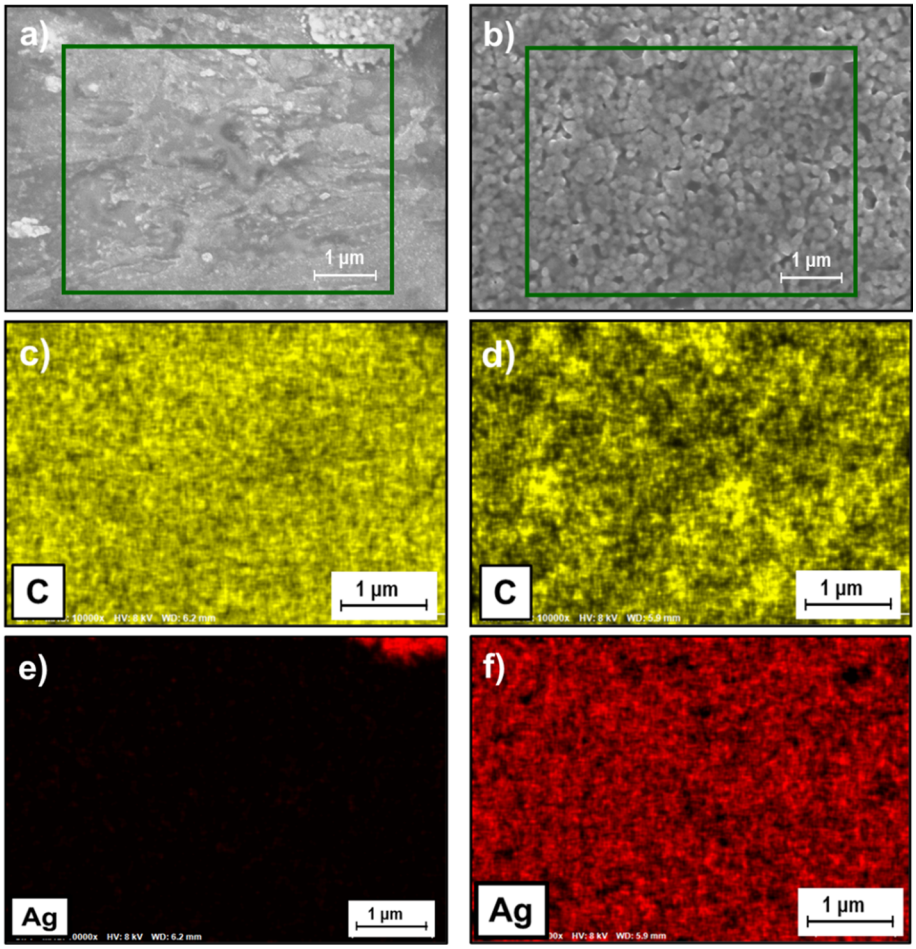

Figure 2 Surface morphologies of PANI films and corresponding EDS elemental carbon and silver maps in between **a**, **c**, **e** and on **b**, **d**, **f** the IDEs. Elemental mappings are acquired from the boxed regions marked in parts (**a**) and (**b**).

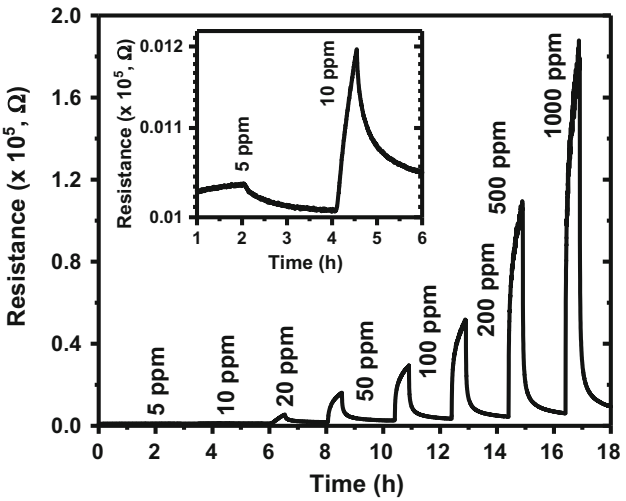

Figure 3 Dynamic resistance transients of PANI-based sensor. Inset shows the response at 5 and 10 ppm NH_3 exposure.

Initially, the resistance of the device is roughly 10^3 Ω that increases by over two orders of magnitude as NH_3 levels increase to 1000 ppm. At 100 mV, this resistance results in very low power consumption of 10 μW or less. For each pulse of NH_3, the resistance of the sensor first increases rapidly and then asymptotically climbs. When the gas flow is stopped, an initial fast drop in resistance is followed by a slow exponential decrease back to baseline. The observed increase in resistance after exposure to NH_3 is ascribed to the adsorption of the gas which triggers deprotonation of ES-PANI, progressively rendering the polymer non-conductive. This process is reversible: as NH_4^+ forms and $DBSA^-$ is freed, the conjugate base of DBSA quickly abstracts a proton from ammonium (PANI-DBSA + NH_3 ⇄ PANI + $DBSA^-$ + NH_4^+) and in turn the acid serves to re-dope EB-PANI back to its original conductive DBSA-PANI form [24]. Note that despite a sudden response upon exposure to NH_3, the longer time intervals toward saturation and recovery may be attributed to the relatively compact (i.e., low surface-to-volume ratio) surface morphology of PANI films on PI substrates. Nevertheless, as can be seen from

the inset of Fig. 3, the sensor detects NH_3 gas in ambient conditions at concentrations as low as 5 ppm, which is comparable or better than the PANI-based or PANI-hybrid sensors reported in the literature [15, 25–28].

In addition, although under dry conditions the response does not reach equilibrium with each 30 min NH_3 exposure, the PANI sensor demonstrates a roughly linear (correlation coefficient, $r^2 = 0.99$) response to higher NH_3 concentrations tested (Fig. 4). Here, the response of the sensor is defined as the normalized change in resistance, $\Delta R_S = (R_G - R_A)/R_A$, and its sensitivity as $S = \Delta R_S/\Delta C_G$, where R_G and R_A represent the resistances of the PANI film in the presence of NH_3 and air, respectively, and C_G denotes the gas concentration. Accordingly, the sensor sensitivity (albeit under non-equilibrium conditions) is expressed by the slope of the line of best fit (18.4×10^{-2}/ppm) to the sensing response versus gas concentration. To derive the detection limit (*DL*) of the sensor, we follow the procedure outlined in previous reports [29] and use the IUPAC definition of *DL* (ppb) as 3× sensor noise/sensitivity [30]. The sensor noise (1.5×10^{-3}) is taken as the variation in the change of normalized resistance at the baseline using the root-mean-square (rms) deviation. Using the definition established above, the *DL* value is estimated as 24 ppb. The observed linear relationship between the sensor response and gas concentration, coupled with low detection limit and low baseline drift, is all highly valuable for the integration of low-cost, low-power sensors on thin polymer platforms. Since selectivity plays a key factor in defining a sensor, the sensitivities of the PANI-based sensor toward other potentially interfering non-Freon refrigerant gases including isobutane (C_4H_{10}) and propane (C_3H_8) at RT are shown in Fig. 5. Corresponding real-time responses are presented in Fig. S4. The sensor demonstrates a specific response to NH_3 gas, exhibiting at least three orders of magnitude higher sensitivity relative to the other refrigerant gases. When corrected for the concentrations tested, the sensitivity ratios toward C_4H_{10} and C_3H_8 to that of 20 ppm NH_3 are 0.09 and 0.06%, respectively.

In terms of repeatability and stability, the printed sensors not only display a low detection limit, but also retain a steady performance over time. Figure 6

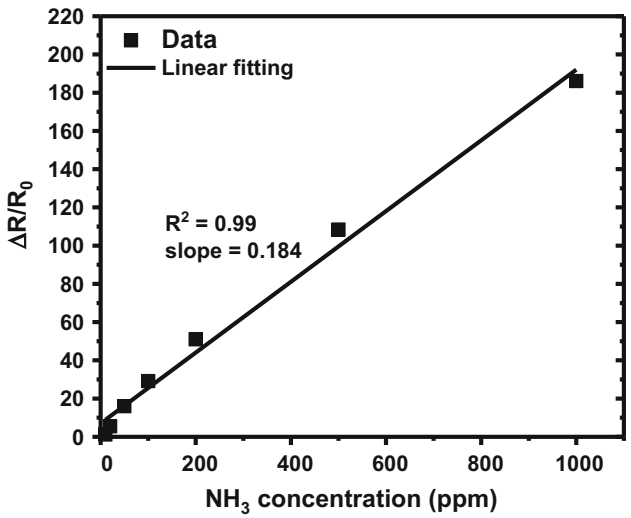

Figure 4 Sensitivity of PANI-based sensor under varying concentrations of NH_3.

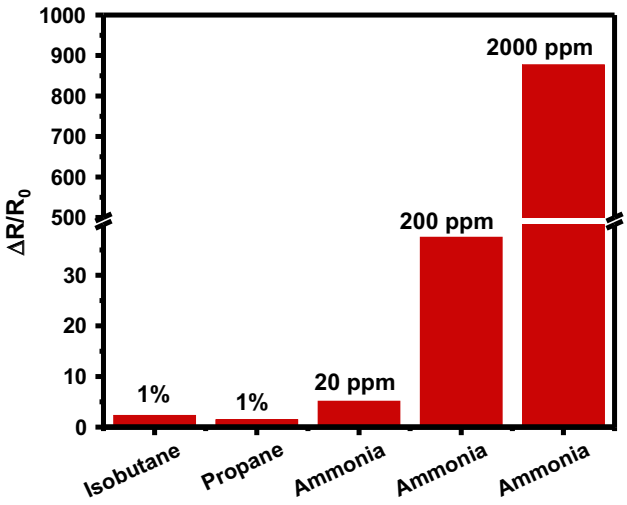

Figure 5 Selectivity of the PANI-based NH_3 sensor toward selected hydrocarbon refrigerants. Note the concentration of both isobutane and propane was kept at a high level of 1% (i.e., 10000 ppm) to enable detection. Sensor response to lower NH_3 concentrations are included for comparison.

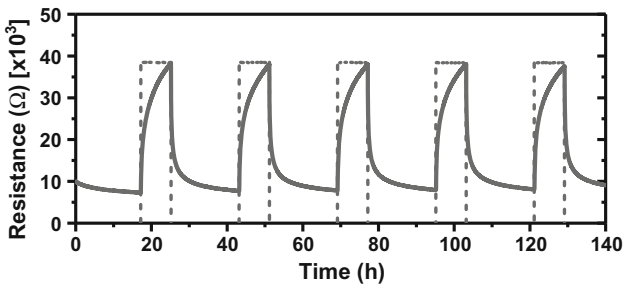

Figure 6 Repeatability of PANI-based sensor following repeated exposures (denoted by the dotted lines) to 20 ppm of NH_3 in dry conditions over 140 h.

illustrates the detection–recovery curves at 20 ppm NH_3 exposures for 8-h followed by 16-h recoveries over an approximate six-day period. As shown, the PANI film is capable of stable gas sensing without a notable loss of functionality. It is also important to note that these data were collected approximately three months after the initial film deposition to elucidate the environmental stability of the fabricated sensors. Our results suggest that exposure at least to ambient laboratory storage conditions does not affect the subsequent performance and functionality of the sensor over an extended time period. The curves demonstrate a complete recovery to baseline resistance with no obvious drift due to a highly reversible reaction between the analyte gas and sensing material. Taken together, these observations point to the excellent stability of all-aerosol-printed PANI-based sensors for at least several months with preservation of full functionality after repeated gas exposures. After a successful laboratory-scale sensor development and performance characterization, long-term reliability evaluation is critical for commercial applications. Interplay of sensor calibration, power consumption, data processing, and communication requirements must be established for a practical manufacturing technology. For refrigeration technology integration, the key sensor requirements of long lifetime (5–10 years), battery powered operation, and wireless communication must be met to address preventive maintenance and deployment requirements which are cost intensive. At the first step, among the sensor technologies of interest for refrigeration application (infrared, electrochemical cell, metal–oxide–semiconductor, catalytic type and heated diode), the printed PANI sensors show promise to meet the cost, sensitivity, size, and low-power requirements. While it remains to be seen whether these sensors will satisfy the common commercial requirement that sensors have a "10-year operational lifetime", the present results are highly promising to further focus on packaging pathways to achieve long-term performance and reliability in the environment of interest.

Response under the influence of humidity and temperature

Next, we test the effect of relative humidity (R_H) by subjecting the same sensor to different R_H levels under varying concentrations of NH_3 (Fig. 7). R_H levels of 30 and 50% are chosen as they represent the typical conditions for indoor and air-conditioned spaces. Comparison of the present sensor responses with earlier studies reveals interesting differences. While Crowley et al. [15] report little interference from humidity, our results are in accordance with responses to humidity previously seen in other PANI-based sensors [31]. Under dry conditions, a fast-initial response to NH_3 is followed by a continual upward drift, resulting in a sluggish stabilization requiring hours. At 30% R_H, a similar steep rise is followed by a smaller downward drift. However, at 50% R_H, stable but notably lower responses are observed at higher NH_3 concentrations as compared to 30% R_H and dry conditions. Most remarkable are the 10%/90% response and recovery to baseline times of roughly 1 min (rise time) and 5 min (recovery time) for both the 30% and 50% R_H values. We speculate that atmospheric water vapor may act as a dispersant for PANI and free DBSA to re-dope and restore the film to its conductive ES-PANI form and thus to stimulate more rapid uptake of NH_3 when humidity is introduced. In fact, the present results corroborate well with observations of increased conductivity in PANI following moisture absorption [32].

On the other hand, for higher concentrations and higher humidity levels (i.e., 50% R_H), the sensor response rapidly stabilizes to a lower sensitivity compared to moisture-free conditions. The observed

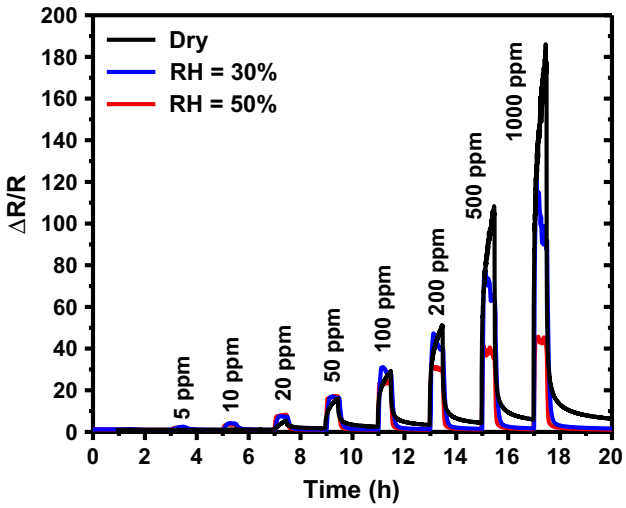

Figure 7 Comparison of the sensing response of PANI-based sensor to various concentrations of NH_3 under different relative humidities.

decrease in resistance with increased R_H is suggested to be related to the increased formation of intermolecular H-bonds between PANI and H_2O, leading to increased charge mobility in the polymer chain [33] (increased hole concentration through donation of the lone pair from the conducting complex toward water molecules) [33–35]. The observed PANI response under the influence of humidity is anticipated considering that humidity has been demonstrated in the literature to influence PANI's conductance and response as previously mentioned. While these observations help elucidate the fundamental facets of PANI's conductivity mechanisms, the exact relationship between humidity interference and PANI-based NH_3 sensing is not entirely clear. As NH_3 readily forms the hydroxide in the presence of moisture, water vapor may generate side reactions with NH_4^+ ions to form NH_4OH. These side reactions with the analyte gas may impact device sensitivity as other basic species (e.g., gaseous amines, triethylamine) can cross-react with PANI and interfere with NH_3 detection [35, 36]. Additionally, the backbone of the polymer may swell upon exposure to moisture, changing the morphological configuration of PANI, thus affecting the film's conductivity and its response to the analyte [35–38]. Although further work is required to fully understand and clarify the underlying interaction mechanisms between PANI and H_2O with respect to NH_3 detection, the sensor remains responsive across the entire concentration range of NH_3 exposures. Future work will explore the long-term stability of devices under varying environmental conditions (e.g., temperature and humidity).

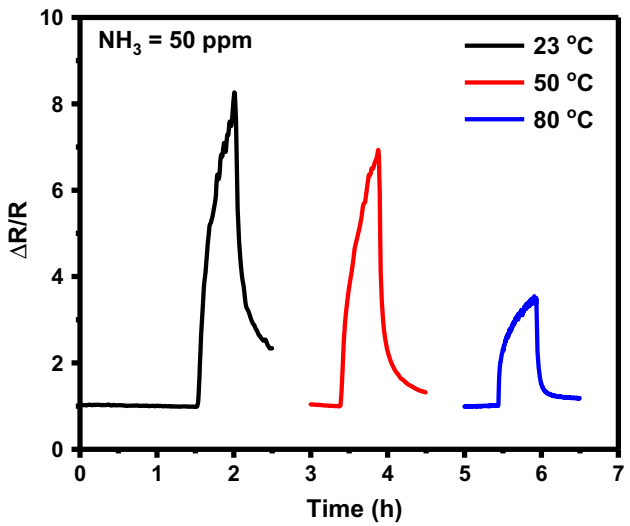

Figure 8 The effect of operating temperature on sensor response to NH_3 gas at a fixed concentration of 50 ppm. The time baseline for each temperature has been offset for clarity.

In addition to humidity, the effect of operating temperature on sensor performance is also evaluated as shown in Fig. 8. It is well known that ES-PANI is less thermally stable with respect to molecular changes than its undoped EB-PANI counterpart. ES-PANI reverts back to EB-PANI upon heating as the doping fraction decreases with increase in temperature [39]. While our experimental conditions likely do not induce degradation of the polymer backbone, conductance of sulfonic acid-doped PANI is known to decrease as temperature increases, sharply dropping off > 160 °C due to loss of the counter-anions and unbound H_2O molecules [39, 40]. While the sensor demonstrates operational functionality from ambient temperatures to 80 °C, as expected, the device's sensitivity toward NH_3 decreases. At 80 °C, the sensor is approximately half as sensitive as operation at RT. In fact, thermal stability studies of PANI-based and PANI-hybrid gas sensors have also reflected our findings of decreasing sensitivity to the analyte gas in the range of 22–48 °C [10, 16, 41, 42]. At elevated temperatures, the conductivity changes in ES-PANI are hypothesized to originate from cross-linkages that drive oxidative condensation reactions between abstracted H^+ units and atmospheric oxygen. Because ES-PANI units can react with oxidants in either physical or electrochemical contact, the degradation of ES-PANI more readily occurs compared to its non-conductive counterpart [43]. In addition to the thermal limitations of unadulterated PANI-based sensors, the binding interactions between PANI and NH_3 may change with respect to temperature, which may result in alterations in the association and dissociation rate constants. Further studies beyond the intended scope of this paper are needed to analyze the reaction kinetics and degradation mechanisms that may interfere with detection responses at elevated temperatures.

Conclusion

We have demonstrated a low-cost, low-power NH_3 gas sensor on PANI-modified IDE arrays accomplished through an additive manufacturing-based technique of aerosol-jet printing. The fabricated

sensors display rapid response, stable repeatability, and excellent selectivity to NH_3 within the desired analytical range of 5–2000 ppm that are all crucial attributes for early leak detection. Our results also reveal the long-term operational potential of these sensors as no notable loss of functionality was observed following three months of exposure to ambient conditions. Additionally, temperature and humidity studies illustrate responsiveness of the sensors at elevated temperatures (80 °C) and/or high humidity levels (50% R_H). When coupled with the potential scalability of the present approach, these results hold great promise toward fabrication of self-powered wireless devices such as facile peel-and-stick toxic gas sensors that can be used in hazardous environments. The direct-write printing approach offers promise for hybrid integration of sensors to achieve the desired sensitivity and selectivity in the application environment while maintaining low-cost and high-volume manufacturability attributes. The additive integration of multiple sensors on the same substrate can lead to an efficient electronic nose platform gaining from the advances in the nanomaterials technology and emerging Internet of Things solutions. Advances in functional inks and printed hybrid electronics are key to the continued development toward a greener future where printed devices may be increasingly deployed and perhaps even become the dominant sensor technology.

Acknowledgements

Research is supported by the US Department of Energy (DOE), Building Technologies Office, under Contract DE-AC05-00OR22725 with UT-Battelle, LLC, for the US DOE. SEM and STEM imaging and analyses were conducted at the Center for Nanophase Materials Sciences (CNMS), which is sponsored at ORNL by the Scientific User Facilities Division, Office of Science, Basic Energy Sciences, US DOE. This manuscript has been authored by UT-Battelle, LLC, under Contract DE-AC05-00OR22725 with the US Department of Energy (DOE). The US government retains and the publisher, by accepting the article for publication, acknowledges that the US government retains a nonexclusive, paid-up, irrevocable, worldwide license to publish or reproduce the published form of this manuscript, or allow others to do so, for US government purposes. DOE will provide public access to these results of federally sponsored research in accordance with the DOE Public Access Plan (http://energy.gov/downloads/doe-public-access-plan).

Author contributions

This work was conceived between TA and PJ and led by TA. Polyaniline synthesis and ink formulation were performed by CF in consultation with KL. Aerosol-jet printing and sensor fabrications were completed by YY. SEM characterizations were performed by LS and KL. Both the gas sensing setup and operation were carried out by B.W. with the assistance of LS. Spectroscopy data were interpreted by CF, imaging data by TA and the gas sensing characterization by BW with the assistance of TA and CF. TS contributed to and participated in the scientific discussion along with all other authors. The original manuscript draft was written by CF and edited by TA and BW. The final manuscript was written through contributions of all authors. All authors have given approval to the final version of the manuscript.

Declarations

Conflict of interest The authors declare that they have no conflict of interest.

Supplementary Information: The online version contains supplementary material available at https://doi.org/10.1007/s10853-021-06080-0.

References

[1] Stratospheric Ozone Protection. U.S. Code, § 7671. Title 42, 2000.

[2] United States Environmental Protection Agency. Phaseout of Class II Ozone-Depleting Substances https://www.epa.gov/ods-phaseout/phaseout-class-ii-ozone-depleting-substances.

[3] Francis C, Maidment G, Davies G (2017) An investigation of refrigerant leakage in commercial refrigeration. Int J Refrig 74:12–21. https://doi.org/10.1016/j.ijrefrig.2016.10.009

[4] Koronaki IP, Cowan D, Maidment G, Beerman K, Schreurs M, Kaar K, Chaer I, Gontarz G, Christodoulaki RI, Cazauran X (2012) Refrigerant emissions and leakage prevention across Europe – results from the realskillseurope project.

Energy 45(1):71–80. https://doi.org/10.1016/j.energy.2012.05.040

[5] Beshr M, Aute V, Sharma V, Abdelaziz O, Fricke B, Radermacher R (2015) A comparative study on the environmental impact of supermarket refrigeration systems using low GWP refrigerants. Int J Refrig 56:154–164. https://doi.org/10.1016/j.ijrefrig.2015.03.025

[6] Joshi, P. Peel and Stick Sensor for Refrigerant Leak Detection https://www.energy.gov/sites/prod/files/2019/05/f62/bto-peer-2019-ornl-peel-stick-sensor-refrig-leak-det.pdf.

[7] Pearson A (2008) Refrigeration with ammonia. Int J Refrig 31(4):545–551. https://doi.org/10.1016/j.ijrefrig.2007.11.011

[8] Harby K (2017) Hydrocarbons and their mixtures as alternatives to environmental unfriendly halogenated refrigerants: an updated overview. Renew Sustain Energy Rev 73:1247–1264. https://doi.org/10.1016/j.rser.2017.02.039

[9] Daniel, J. S.; Velders , G. J. M. Halocarbon Scenarios, Ozone Depletion Potentials, and Global Warming Potentials. In *Scientific Assessment of Zzone Depletion: 2006*; Global Ozone Research and Monitoring Project; World Meteorological Organization: Geneva, Switzerland, 2007; Vol. 50, pp 8.1–8.39.

[10] Pandey S (2016) Highly sensitive and selective chemiresistor gas/vapor sensors based on polyaniline nanocomposite: a comprehensive review. J Sci Adv Mater Devices 1(4):431–453. https://doi.org/10.1016/j.jsamd.2016.10.005

[11] Tanguy NR, Thompson M, Yan N (2018) A review on advances in application of polyaniline for ammonia detection. Sens Actuators B Chem 257:1044–1064. https://doi.org/10.1016/j.snb.2017.11.008

[12] Fratoddi I, Venditti I, Cametti C, Russo MV (2015) Chemiresistive polyaniline-based gas sensors: a mini review. Sens Actuators B Chem 220:534–548. https://doi.org/10.1016/j.snb.2015.05.107

[13] Molapo KM, Ndangili PM, Ajayi RF, Mbambisa G, Mailu SM, Njomo N, Masikini M, Baker P, Iwuoha EI (2012) Electronics of conjugated polymers (I): polyaniline. Int J Electrochem Sci 7:11859–11875

[14] Liao G, Li Q, Xu Z (2019) The chemical modification of polyaniline with enhanced properties: a review. Prog Org Coat 126:35–43. https://doi.org/10.1016/j.porgcoat.2018.10.018

[15] Crowley K, Morrin A, Hernandez A, O'Malley E, Whitten PG, Wallace GG, Smyth MR, Killard AJ (2008) Fabrication of an ammonia gas sensor using inkjet-printed polyaniline nanoparticles. Talanta 77(2):710–717. https://doi.org/10.1016/j.talanta.2008.07.022

[16] Rizzo G, Arena A, Donato N, Latino M, Saitta G, Bonavita A, Neri G (2010) Flexible, all-organic ammonia sensor based on dodecylbenzene sulfonic acid-doped polyaniline films. Thin Solid Films 518(23):7133–7137. https://doi.org/10.1016/j.tsf.2010.07.016

[17] Crowley K, O'Malley E, Morrin A, Smyth MR, Killard AJ (2008) An Aqueous ammonia sensor based on an inkjet-printed polyaniline nanoparticle-modified electrode. Analyst 133(3):391–399. https://doi.org/10.1039/B716154A

[18] Huang Q, Zhu Y (2019) Printing Conductive Nanomaterials for Flexible and Stretchable Electronics: A Review of Materials, Processes, and Applications. Adv Mater Technol 4(5):1800546. https://doi.org/10.1002/admt.201800546

[19] Kuswandi B, Jayus M, Restyana A, Abdullah A, Heng LY, Ahmad MA (2012) Novel colorimetric food package label for fish spoilage based on polyaniline film. Food Control 25(1):184–189. https://doi.org/10.1016/j.foodcont.2011.10.008

[20] Le Maout P, Wojkiewicz JL, Redon N, Lahuec C, Seguin F, Dupont L, Mikhaylov S, Noskov Y, Ogurtsov N, Pud A (2018) Polyaniline nanocomposites based sensor array for breath ammonia analysis. Portable e-Nose approach to non-invasive diagnosis of chronic kidney disease. Sens Actuators B Chem 274:616–626. https://doi.org/10.1016/j.snb.2018.07.178

[21] Haynes, A.; Gouma, P.-I. Polyaniline-Based Environmental Gas Sensors. In *Sensors for Environment, Health and Security*; Baraton, M.I., Ed.; NATO Science for Peace and Security Series C: Environmental Security; Springer Netherlands: Dordrecht, 2009; pp 451–459. https://doi.org/https://doi.org/10.1007/978-1-4020-9009-7_30.

[22] Moulton SE, Innis PC, Kane-Maguire LAP, Ngamna O, Wallace GG (2004) Polymerisation and characterisation of conducting polyaniline nanoparticle dispersions. Curr Appl Phys 4(2):402–406. https://doi.org/10.1016/j.cap.2003.11.059

[23] Ngamna O, Morrin A, Killard AJ, Moulton SE, Smyth MR, Wallace GG (2007) Inkjet printable polyaniline nanoformulations. Langmuir ACS J Surf Colloids 23(16):8569–8574. https://doi.org/10.1021/la700540g

[24] Huang, J.; Kaner, R. B. Polyaniline nanofibers: Syntheses, properties, and applications. In *Conjugated Polymers: Theory, Synthesis, Properties, and Characterization*; CRC Press: Boca Raton, FL, 2007; Vol. 1, pp 7.1–7.49.

[25] Deshpande NG, Gudage YG, Sharma R, Vyas JC, Kim JB, Lee YP (2009) Studies on tin oxide-intercalated polyaniline nanocomposite for ammonia gas sensing applications. Sens Actuators B Chem 138(1):76–84. https://doi.org/10.1016/j.snb.2009.02.012

[26] Tai H, Jiang Y, Xie G, Yu J (2010) Preparation, characterization and comparative NH_3-sensing characteristic studies of pani/inorganic oxides nanocomposite thin films. J Mater Sci

Technol 26(7):605–613. https://doi.org/10.1016/S1005-0302(10)60093-X

[27] Gavgani JN, Hasani A, Nouri M, Mahyari M, Salehi A (2016) Highly sensitive and flexible ammonia sensor based on S and N Co-doped graphene quantum dots/polyaniline hybrid at room temperature. Sens Actuators B Chem 229:239–248. https://doi.org/10.1016/j.snb.2016.01.086

[28] Pang Z, Yang Z, Chen Y, Zhang J, Wang Q, Huang F, Wei Q (2016) A room temperature ammonia gas sensor based on cellulose/TiO_2/PANI composite nanofibers. Colloids Surf Physicochem Eng Asp 494:248–255. https://doi.org/10.1016/j.colsurfa.2016.01.024

[29] Li J, Lu Y, Ye Q, Cinke M, Han J, Meyyappan M (2003) Carbon Nanotube sensors for gas and organic vapor detection. Nano Lett 3(7):929–933. https://doi.org/10.1021/nl034220x

[30] Currie LA (1999) Nomenclature in evaluation of analytical methods including detection and quantification capabilities: (IUPAC recommendations 1995). Anal Chim Acta 391(2):105–126. https://doi.org/10.1016/S0003-2670(99)00104-X

[31] Grigore L, Petty MC (2003) Polyaniline films deposited by anodic polymerization: properties and applications to chemical sensing. J Mater Sci Mater Electron 14(5):389–392. https://doi.org/10.1023/A:1023908903260

[32] Kumar L, Rawal I, Kaur A, Annapoorni S (2017) Flexible room temperature ammonia sensor based on polyaniline. Sens Actuators B Chem 240:408–416. https://doi.org/10.1016/j.snb.2016.08.173

[33] Kulkarni MV, Apte SK, Naik SD, Ambekar JD, Kale BB (2013) Ink-Jet printed conducting polyaniline based flexible humidity sensor. Sens Actuators B Chem 178:140–143. https://doi.org/10.1016/j.snb.2012.12.046

[34] Zhang Y, Duan Y, Liu J (2017) The effect of intermolecular hydrogen bonding on the polyaniline water complex. J Clust Sci 28(3):1071–1081. https://doi.org/10.1007/s10876-016-1104-x

[35] Kulkarni MV, Viswanath AK (2007) Sulphonic acids doped Poly(N-Ethyl Aniline): a material for humidity sensing application. Polym Eng Sci 47(10):1621–1629. https://doi.org/10.1002/pen.20838

[36] Mikhaylov S, Ogurtsov N, Noskov Y, Redon N, Coddeville P, Wojkiewicz JL, Pud A (2015) Ammonia/Amine electronic gas sensors based on hybrid Polyaniline–TiO2 nanocomposites. The effects of titania and the surface active doping acid. RSC Adv. 5(26):20218–20226. https://doi.org/10.1039/C4RA16121A

[37] Wang J, Chan S, Carlson RR, Luo Y, Ge G, Ries RS, Heath JR, Tseng H-R (2004) Electrochemically fabricated polyaniline nanoframework electrode junctions that function as resistive sensors. Nano Lett 4(9):1693–1697. https://doi.org/10.1021/nl049114p

[38] Cho S, Lee JS, Joo H (2019) Recent developments of the solution-processable and highly conductive polyaniline composites for optical and electrochemical applications. Polymers 11(12):1965. https://doi.org/10.3390/polym11121965

[39] Yue J, Epstein AJ, Zhong Z, Gallagher PK, Macdiarmid AG (1991) Thermal stabilities of polyanilines. Synth Met 41(1–2):765–768. https://doi.org/10.1016/0379-6779(91)91180-I

[40] Chen T, Dong C, Li X, Gao J (2009) Thermal degradation mechanism of dodecylbenzene sulfonic acid- hydrochloric acid co-doped polyaniline. Polym Degrad Stab 94(10):1788–1794. https://doi.org/10.1016/j.polymdegradstab.2009.06.011

[41] Patil PT, Anwane RS, Kondawar SB (2015) Development of Electrospun Polyaniline/ZnO composite nanofibers for LPG sensing. Procedia Mater Sci 10:195–204. https://doi.org/10.1016/j.mspro.2015.06.041

[42] Sharma HJ, Jamkar DV, Kondawar SB (2015) Electrospun nanofibers of conducting Polyaniline/Al-SnO_2 composites for hydrogen sensing applications. Procedia Mater Sci 10:186–194. https://doi.org/10.1016/j.mspro.2015.06.040

[43] Šeděnková I, Trchová M, Stejskal J (2008) Thermal degradation of polyaniline films prepared in solutions of strong and weak acids and in water – FTIR and raman spectroscopic studies. Polym Degrad Stab 93(12):2147–2157. https://doi.org/10.1016/j.polymdegradstab.2008.08.007